

Turbulence – Obstacle Interactions in the Lagrangian Framework: Applications for Stochastic Modeling in Canopy Flows*

Ron Shnapp,[†] Yardena Bohbot-Raviv,[‡] Alex Liberzon,[†] and Eyal Fattal[‡]

Lagrangian stochastic models are widely used for making predictions and in the analysis of turbulent dispersion in complex environments, such as the terrestrial canopy flows. However, due to a lack of empirical data, it is still not known how particular features of canopy phenomena affect the parameterizations of Lagrangian statistics. In the following work, we consider the impact of obstacle wakes on Lagrangian statistics. Our analysis is based on 3D trajectories measured in a wind-tunnel canopy flow model, where we estimated Lagrangian statistics directly. In particular, we found that both the Lagrangian autocorrelation and the second order structure functions could be well represented using a second-order Lagrangian stochastic model. Furthermore, a comparison of our empirically estimated statistics with predictions for the case of homogeneous flow shows that decorrelation times of Lagrangian velocity were very short and that the Kolmogorov constant, C_0 , was not a function of Re_λ alone in our canopy flow. Our subsequent analysis indicated that this was not a result of flow inhomogeneity, but instead a result of the wake production. Thus, our empirical study suggests that the wake-production can lead to a so-called “rapid decorrelation” in which both C_0 and the separation of scales T/τ_η (T being a Lagrangian velocity decorrelation timescale) are not determined by Re_λ alone, and may cause finite Reynolds number effects to occur even at high Reynolds number canopy flows.

I. INTRODUCTION

Dispersion of scalars in the atmospheric surface layer is strongly influenced by turbulent canopy flows. This critical physical process affects the dispersal of pathogens and the ventilation in urban areas [1], and the dispersal of spores, bacteria and seeds in forests and fields [2]. It had become commonly accepted that there is a specific difficulty to estimate dispersion in canopy flows through the Eulerian framework, resulting from the failure of gradient-diffusion theory in these flows, e.g. Refs. [3–5]. Consequently, the Lagrangian Stochastic Models (LSM) gained popularity as an alternative modeling approach within the community (e.g. Refs. [2, 6–16] among others). The LSMs can efficiently predict transport and dispersion in turbulent flows through Monte-Carlo simulations [8], and are specifically useful in applications to inhomogeneous turbulence (i.e. where the flow statistics vary in space) and to cases with a complex source distribution.

In the LSM, a stochastic Markov random walk provides increments of the states of “marked” particles, defined by the particles’ positions and the set of its time derivatives $\{\frac{d^i \mathbf{x}}{dt^i}\}$, $i = 0, 1, \dots, n$ (usually $n = 1$ or $n = 2$ is the order of the model, and boldfaced symbols denote vectors). In the case of $n = 1$, the main assumption, attributed to Obukhov [17], is that at infinite Reynolds numbers the particle acceleration can be considered local in time and space, and thus, an uncorrelated random forcing can be assumed in the inertial range. Obukhov’s formal approach provides a theoretical framework for modeling, in principle any stationary turbulent flow, provided that the time steps are in the inertial subrange (this has since been supported by experimental work, see in particular Ref. [18]). In order to solve the Fokker-Plank equation for turbulent flows in practice, the first order damping term has to be solved. Another important step was formulated by Thomson [19] with the introduction of the well-mixed principle, enabling to determine the damping function by using a prescribed Eulerian velocity PDF. Although the well-mixed principle severely constraints the damping function for general anisotropic inhomogeneous turbulence, a general solution (except for the one dimensional case [20]) could not be derived. This is known as the non-uniqueness problem [21–23].

The LSM does not account for the statistics of the flow field, so a main challenge in the construction of LSMs lies in the ability of the calculated paths to represent trajectories of fluid parcels. In particular, one has to supply the Eulerian single point velocities PDFs, information on the Lagrangian integral timescale, and their dependence on the particular inhomogeneity of the specific type of canopy. In the case of canopy flows, there is a number of issues that require special attention:

* ronshnapp@gmail.com

[†] School of Mechanical Engineering, Tel Aviv University, Tel Aviv, Israel

[‡] Israel Institute for Biological Research, Ness Ziona, Israel

1. turbulence generated by both the large scale shear and due to flow–obstacle interactions (wakes) of canopy elements, leading to so-called spectral short-circuiting through wake–production [24];
2. inhomogeneity due to the significant difference between the flow above and inside the canopy layer, leading to a strong shear layer above the canopy;
3. the prevalence of large coherent structures in the shear layer, so-called mixing layer analogy [25];
4. non Gaussian distributions of turbulent statistics, characterized by skewed PDFs of the Eulerian single-point velocity [24, 26];
5. the “mechanical diffusion” as a result of the fluid having to bypass the canopy obstacles [27] (similar to the dispersion in porous media flows);

It is therefore of the great importance to understand how items 1-5 can be addressed by LSMs. This work addresses small scale motion in the wake of canopy obstacles, namely we focus here on item 1.

Numerous attempts were presented in the past to overcome the above difficulties; let us present several examples of such studies, which by no means can be a conclusive list due to a very large body of literature. Thomson’s [19] so-called ‘simplest-solution’ provided a first-order LSM that uses inhomogeneous flow statistics, and has been widely used in canopy flows, e.g. Refs. [10, 28, 29], among others. It is not the only successful LSM for canopy flows, as was demonstrated for instance by Reynolds [30]. The influence of the coherent structures, short-circuiting or skewed PDFs on the Lagrangian statistics is not yet understood, e.g. [7, 15, 31]. Studies have shown that different parameterizations of the flow statistics (e.g. the specific profile of the dissipation rate or the Lagrangian time scale, introduced below) have strong effect on the accuracy of LSM predictions [28, 31–33]. Nevertheless, direct estimations of Lagrangian flow statistics in canopy flows that could provide this crucial data are lacking. The influence of the turbulence–obstacle interaction on the Lagrangian statistics in the canopy flow was not addressed directly in the past, which forms the focus of this work.

Technological and scientific advances of the last two decades enabled gathering of invaluable empirical data in the Lagrangian framework, both through experiments and direct numerical simulations (e.g. Refs. [34–53]). Such studies have analyzed the details of Lagrangian motion, bringing attention in the community to delicate mechanisms underlying the motion of Lagrangian particles in turbulent flows [47]. The empirical data obtained in such studies can be used to bridge the gap between the fluid mechanics and the stochastic models through more accurate parameterizations or validation of theories. In most cases, due to practical limitations, the focus was put on homogeneous isotropic turbulent flows (HIT); however, it appears that studies with embedded inhomogeneity and anisotropy are gaining forward momentum in the recent years (e.g. Refs. [50–52, 54–56]).

In this study we use measurements of flow tracers in a wind tunnel model of a heterogeneous canopy flow [56, 57] to better understand the effect of flow–obstacle interactions on Lagrangian statistics (item 1). This process “short-circuits” the turbulent kinetic energy in the canopy layer: turbulent kinetic energy is extracted from large scales (of the order of canopy height, H) and injected at small scales (of the order of obstacle thickness) [24], in addition to turbulent kinetic energy created from the mean shear with inhomogeneity through the Richardson-Kolmogorov cascade [58]. Poggi et al. [33] have already shown analytically that wake-production can alter the value of the Kolmogorov constant C_0 which, in some sense, characterizes the cascade process. Our analysis, made experimentally and directly in the Lagrangian framework, is used to estimate crucial Lagrangian statistics, and thus allows better insight on turbulent dynamics inside the canopy. Specifically, we focus on the small scales and compare our results with homogeneous turbulence cases to reveal the influence of wake production on Lagrangian statistics.

II. METHODS

A. Definitions

The simplest first order LSM, assuming a homogeneous turbulent flow with zero mean Gaussian velocity PDFs at each point (hereafter called Gaussian turbulence), is the Ornstein-Uhlenbeck (OU) process [59] –

$$\begin{aligned} dv_i &= \alpha_i(x, v, t) dt + \beta_i(x, v, t) d\xi_i \quad ; \quad dx_i = v_i(\tau) d\tau \\ \alpha_i &= -\frac{v_i}{T_L} \quad ; \quad \beta_i = \left(\frac{2\sigma_i^2}{T_L}\right)^{1/2}. \end{aligned} \quad (1)$$

Here v_i is the i_{th} component of the velocity of a Lagrangian particle, $d\xi_i$ are increment components of a Wiener process, and σ_i is the standard deviation of v_i . The Lagrangian velocity autocorrelation function, ρ_{ij} , and the Lagrangian integral timescale, $T_{L,i}$, are defined as –

$$\rho_{ij}(\tau) = \frac{\langle v_i(0) v_j(\tau) \rangle}{\langle v_i^2(0) \rangle^{1/2} \langle v_j^2(\tau) \rangle^{1/2}} \quad ; \quad T_{L,i} = \int_0^\infty \rho_{ii}(\tau) d\tau \quad (2)$$

where angular brackets $\langle \cdot \rangle$ denote an average, the velocities $v_i(0) v_j(\tau)$ are taken along an individual Lagrangian trajectory, and since we are considering a homogeneous and stationary flow, $\rho_{ij}(\tau)$ is a function of τ only. Doob [60] proved that the OU process, Eq. (1), is essentially the only process defined with the properties: stationary, Gaussian and Markovian, with an exponential autocorrelation function:

$$\rho_{ij}(\tau) = \delta_{ij} \exp\left(-\frac{\tau}{T_{L,i}}\right). \quad (3)$$

Furthermore, based on the Obukhov conjecture [17], consistency with Kolmogorov inertial range scaling of Lagrangian velocity increments [61] in the model requires that [8] –

$$\frac{2\sigma_i^2}{T_{L,i}} = \frac{D_{ii}(\tau)}{\tau} = C_0 \epsilon \quad ; \quad D_{ii}(\tau) = \langle [v_i(\tau) - v_i(0)]^2 \rangle \quad (4)$$

where $D_{ii}(\tau)$ is termed the Lagrangian second order structure function, C_0 is the so-called Kolmogorov constant, and ϵ is the mean rate of turbulent kinetic energy dissipation. Borgas and Sawford [20] showed that for HIT these choices of α_i , β_i are unique solutions of Thomson's well-mixed condition [19].

Thus far we have only considered first order LSMs ($n = 1$) that are regarded accurate in flows with very high Reynolds numbers. In such cases the particle accelerations have very short correlation times relative to the integral timescales [34, 35, 61]. However, as the Reynolds number decreases, this separation of timescales reduces and the above approximation becomes inaccurate. The influence of finite separation of scales (through finite Reynolds number) was addressed in Sawford's second order model ($n = 2$) for the HIT case [62] –

$$\begin{aligned} T_L da_i + (1 + R^{1/2}) a_i(t) dt + \frac{R^{1/2}}{T_L} \int_0^t a_i(\tau) d\tau dt &= \sqrt{\frac{2\sigma}{T_L} R^{1/2} (1 + R^{-1/2})} d\xi_i \\ dv_i &= a_i d\tau \quad ; \quad dx_i = v_i d\tau \quad ; \quad R = \frac{16a_0^2}{C_0^4} \left(\frac{\tau_e}{\tau_\eta}\right)^2 \end{aligned} \quad (5)$$

where a_0 is a Kolmogorov constant for the variance of acceleration, \mathbf{a} is a particle's acceleration, τ_e is an Eulerian integral timescale and $\tau_\eta = (\nu/\epsilon)^{1/2}$ is the Kolmogorov timescale, and R is a Reynolds number. The model Eq. (5) has the corresponding velocity autocorrelation function [62] –

$$\rho_{ij}(\tau) = \delta_{ij} \frac{T_1 \exp(-\tau/T_2) - T_2 \exp(-\tau/T_1)}{T_1 - T_2} \quad ; \quad T_L = T_1 + T_2. \quad (6)$$

This second order model was extended by Du et al. [63] to the decaying turbulence case and by Reynolds [64] to include vertical inhomogeneity of the turbulent flow statistics.

The above two LSMs, Eq. (1) and (5), were used in the analysis of the experimental results. They were chosen specifically for their simplicity so as to achieve a clear interpretation of our results.

B. Experimental Method

In our investigation, we used the results from a wind-tunnel experiment. Detailed descriptions of the experimental apparatus, measurements, and post processing, were given in Refs. [56, 57], yet for completeness, we present a brief overview here also. The environmental wind-tunnel laboratory at IIBR features a 14 meters long open wind-tunnel with a $2 \times 2 \text{ m}^2$ cross sectional area, that is compatible for conducting experiments mimicking turbulent flows in the atmospheric surface layer. The canopy flow was modeled by placing flat rectangular plates on the bottom wall of the wind tunnel. We used two types of plates with a height of either H or $\frac{1}{2}H$, and a width of $\frac{1}{2}H$, where $H = 100 \text{ mm}$. The two types of plates were positioned in consecutive rows and at a staggered orientation, see Fig 1(a). The entire upstream part of the test section was fitted with roughness elements. The canopy frontal area density, defined as $\Lambda_f = A_f/A_T$, (A_f being is the element frontal area, and A_T the lot area of the canopy) was $9/16$.

Data was gathered at two levels of the free stream velocity, corresponding to Reynolds numbers $Re_\infty \equiv U_\infty H/\nu = 16 \times 10^3$ and 26×10^3 ; with $U_\infty = 2.5$ and 4 m s^{-1} being the free stream mean velocity measured with a sonic anemometer at the center of the wind-tunnel cross section, and ν the kinematic viscosity of the air. In what follows we adopt the frame of reference commonly used in the canopy flow literature – x is streamwise aligned longitudinally within the wind-tunnel, y is horizontal cross-stream direction, and z is directed vertically away from the bottom wall with the plane $z = 0$ corresponding to the bottom wall.

In the experiment we have tracked the positions of fluid tracers using a real-time extension of the 3D-PTV method [56]. The flow was seeded with hollow glass spheres of diameter 5 micrometer on average, with the Stokes number $St = \tau_p/\tau_\eta \approx 0.05$. The tracers were illuminated with a 10W, 532nm continuous wave laser; 3D positions were inferred from 4 Mega pixel images at a resolution of $50 \text{ }\mu\text{m}$ per pixel and rates of 500 Hz within the canopy layer $z \leq H$, and 1000 Hz above the elements $z > H$. We implemented camera calibration, stereo matching and tracking [65], to reconstruct the tracer particle’s trajectories by using the OpenPTV [66] open source software, integrated to operate with the real-time image analysis extension. The trajectory data analysis was performed by employing our open source Flowtracks package [67].

C. The Sub-Volume Approach

We analyzed trajectories at different locations in 20 sub-volumes, which are rectangular cuboids found at 4 horizontal locations, and at 5 different heights above the wind-tunnel bottom wall. Sub-volume horizontal positions are labeled alphabetically a , b , c and d ; a is found immediately downstream of a tall element, b is upstream to the next tall element, and c and d are parallel to the former elements and positioned around a short element, see diagram in Fig. 1(a). At each position, $a - d$, we used 5 vertical slabs of thickness $0.2H$ to define the sub-volumes; the vertical slab position is labeled numerically 1-5 and corresponds to heights $0.5-0.7$, $0.7-0.9$, $0.9-1.1$, $1.1-1.3$ and $1.3-1.5H$, respectively. Thus, for example, the sub-volume $b2$ was found upstream of a tall element and occupied the range $0.7H < z < 0.9H$. An animation of a sub-sample from our data set can be seen online through the link [68].

Lagrangian statistics are commonly represented based on a common point of origin (x_0, t_0) and as a function of time [61]. Thus the Lagrangian mean of an arbitrary function $\langle A(x_0, t_0, t) \rangle$, is normally defined over flow ensembles. In this work we assume that the flow is stationary (see [56]) and ergodic, and thus we replace the above with an average over t_0 , presented as a function of time lag $\tau = t - t_0$, where t_0 is the time a particle was first spotted on our measurements. In addition, we present statistics for all the particles crossing a sub-volume of space. The procedure implies an assumption of a locally homogeneous flow across the size of each sub-volume, which is small compared to the roughness elements that was verified to dictate the spatial variations of flow statistics. Therefore, the ensemble average over sub-volume \mathbb{V} , $\langle A \rangle_v$ of any quantity A , is calculated as –

$$\langle A(\mathbf{x}, \tau) \rangle_v \equiv \frac{1}{N} \sum_{i=0}^N A_i(\mathbf{x}_v, \tau) \quad (7)$$

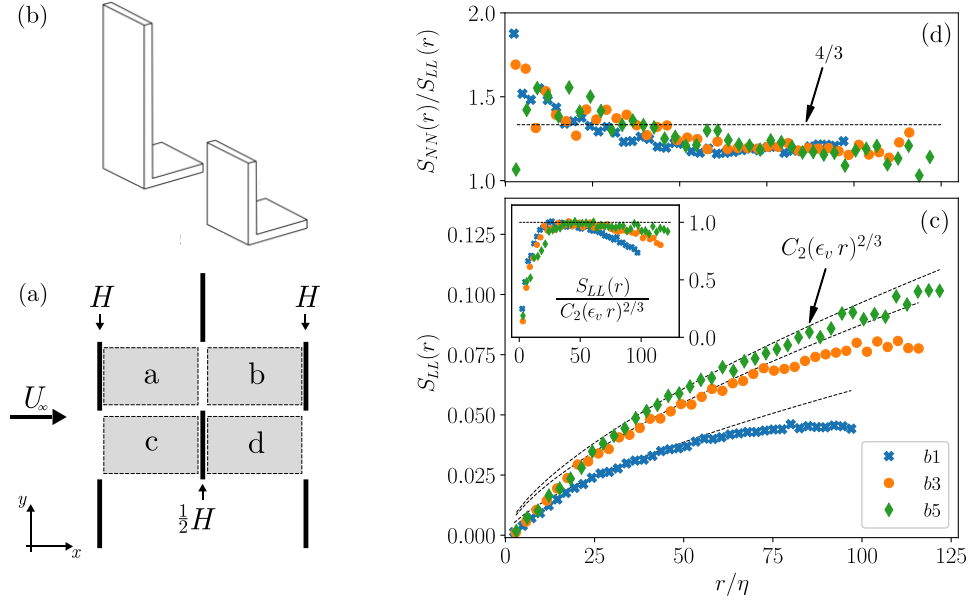


Figure 1: (a) A top view sketch of the canopy repeating unit cell. Grey shaded regions show the positions of the four groups of sub-volumes. Black thin rectangles represent the canopy roughness elements. (b) An isometric sketch of the short and tall roughness obstacles used. (c) Main panel shows the second order Eulerian longitudinal structure function in three sub-volumes, and dashed lines show the isotropic model, Eq. (8), with the estimated values ϵ_v . The inset shows the compensated structure functions for the same cases. (d) The ratio between the longitudinal and the transverse Eulerian structure functions, compared with the k41 isotropic $4/3$.

such that \mathbf{x}_v are positions of Lagrangian tracers inside the sub-volume $\mathbf{x}_v \in \mathbb{V}$, and N is the number of the Lagrangian trajectories in the sub-volume over the time of experiment. For brevity, the subscript will be omitted, and the sub-volume regarded will be stated clearly in the text, figure legends, and captions.

D. Mean Rate of Dissipation

The Eulerian second order structure function is defined as the second moment of spatial velocity differences $\delta \mathbf{u}'_r \equiv \mathbf{u}'(\mathbf{x}) - \mathbf{u}'(\mathbf{x} + \mathbf{r})$ [61]. Assuming local isotropy and homogeneity, the Kolmogorov universal similarity theory [69] predicts that the longitudinal component of the second order structure function, S_{LL} , and its transverse component, S_{NN} , (i.e. the components aligned with \mathbf{r} or normal to \mathbf{r} respectively) admit to the following scaling law in the inertial range of scales –

$$\begin{aligned}
 S_{LL}(\mathbf{x}, r) &= \left\langle \left(\delta \mathbf{u}'_r \cdot \frac{\mathbf{r}}{r} \right)^2 \right\rangle = C_2 (\epsilon r)^{2/3} \\
 S_{NN}(\mathbf{x}, r) &= \frac{1}{2} \left(\langle \delta \mathbf{v}^2(\mathbf{r}) \rangle - S_{LL}(r) \right) = \frac{4}{3} C_2 (\epsilon r)^{2/3}
 \end{aligned} \tag{8}$$

where in the homogeneous turbulence case the \mathbf{x} dependence drops, $r = |\mathbf{r}|$, and $C_2 \approx 2.1$ is a supposedly universal constant [70].

We implemented Eq. (8) to estimate S_{LL} in each sub-volume, using the Lagrangian dataset and averaging velocity differences over spherical shells, as was done in Refs. [36, 53]. This gives a structure function that is isotropic by construction, namely it depends only on the distance r . For example, in the main panel of Fig. 1(c) we present our estimations of $S_{LL}(r)$ in the sub-volumes b1, b3 and b5 for the $Re_\infty = 16 \times 10^3$ case. Note that our estimation of S_{LL} does not use the Taylor's hypothesis.

Using S_{LL} we estimated an empirical mean rate of dissipation in each sub-volume. Since S_{LL} is quadratic

with r in the dissipation range and should change very slowly at large scales above the integral scale [61], the compensated structure functions $S_{LL}(r)/C_2(\epsilon r)^{2/3}$ should peak in the intermediate range $\eta < r < \mathcal{L}$, and this is shown in the inset of Fig. 1(c). Thus, we defined a sub-volume averaged dissipation rate as

$$\epsilon_v \equiv \max_r \left[\frac{S_{LL}(r)}{C_2 r^{2/3}} \right] \quad (9)$$

where S_{LL} is estimated with samples $\mathbf{x} \in \mathbb{V}$. Using Eq. (9) instead of a least square fitting has the advantage of not having to specify a range of r where an inertial range scaling supposedly exists; on the other hand, it may overestimate the value that would have been obtained in a fitting process, but this uncertainty is low (arguably much lower than the uncertainty in the value of C_2). Also, due to anisotropy and inhomogeneity, the applicability of Eq. (8) to canopy flow turbulence is not straightforward, for example as observed in Refs. [28, 71, 72]. Nevertheless, in Fig. 1(b) we compare our estimation of $S_{LL}(r)$ with Eq. (8) using ϵ_v , and for all cases we observe a distinct range of r , where a good agreement is achieved between the theory and the empirical data. In addition to that, the transverse components, S_{NN} were similarly estimated using Eq. (8) and the Lagrangian dataset. The ratios S_{NN}/S_{LL} were calculated and an example is shown in Fig. 1(d) as a function of r for the three sub-volumes b1, b3, and b5. The ratios are compared in the figure to the K41 isotropic value of $S_{NN} = \frac{4}{3}S_{LL}$ [69]. The figure shows that S_{NN}/S_{LL} decreases with r and that in the region where S_{LL} agrees with the inertial range scaling $S_{NN} \approx \frac{4}{3}S_{LL}$. These observations of agreement with K41 similarity in a certain range of r support the use of ϵ_v as a parameterization in our experiment. Therefore, in analogy to the usual case, sub-volume averaged dissipation scales were calculated as $\eta \equiv (\nu^3/\epsilon_v)^{1/4}$ and $\tau_\eta \equiv (\nu/\epsilon_v)^{1/2}$, being the length and time scales respectively.

With the estimations of ϵ_v , a Taylor microscale Reynolds number is defined as –

$$Re_{\lambda,v} \equiv v'^2 \left(\frac{15}{\epsilon_v \nu} \right)^{1/2} \quad (10)$$

where $v'^2 = \langle \sum_i (v_i - U_i)^2 \rangle$ is the RMS of particle velocity relative to the sub-volume averaged velocity, $U_i = \langle v_i \rangle$. Estimations of ϵ_v and $Re_{\lambda,v}$ were repeated for all sub-volumes and the values are tabulated in the Appendix. The Reynolds numbers $Re_{\lambda,v}$ are in the range 350-850, with practically negligible dependence on Re_∞ . The obtained values were used for parameterization of the results presented below and the subscript “ v ” is omitted to facilitate readability.

III. DIRECT ESTIMATION OF LSM PARAMETERS

In this section we use the wind-tunnel Lagrangian dataset in order to extract two critical LSM parameters: the Lagrangian velocity decorrelation time scale and the Kolmogorov constant, C_0 . To do so we calculate the autocorrelation and the structure functions and directly extract the two parameters using their definitions.

A. Lagrangian Autocorrelation and Decorrelation Timescale

We estimated the Lagrangian autocorrelation functions using a formula equivalent to Eq.(2.6) in the paper by Guala et al. [44] with the ensemble averaging Eq. (7), as presented and discussed in Appendix B. Fig. 2(a) presents ρ_{ii} for the three components of Lagrangian velocity in sub-volume b3. For all three components, a concave shape is seen at the origin, reminiscent of a parabolic decrease at small delay times, providing the way to estimate the Taylor micro-timescale [73]. The autocorrelation functions decrease monotonically with the increasing time lag, τ . The rate of decrease is roughly the same for ρ_{xx} and ρ_{yy} , whereas the decrease is faster for the vertical component, ρ_{zz} . These observations were robust throughout all of the sub-volumes and the two Re_∞ cases.

The Lagrangian autocorrelation function $\rho_{ii}(\tau)$ does not decrease to zero within the range of our measurements, which is due to the high mean flow velocity and finite size of the measurement volume between two rows of obstacles. Therefore, we cannot directly use the integral in Eq. (2) to estimate the $T_{L,i}$. Similarly to other Lagrangian measurements (Refs. [41, 74]), we define a Lagrangian *decorrelation timescale*, T_i , by fitting a model for ρ_{ii} within the available range of the data. Specifically, we used a least square minimization to

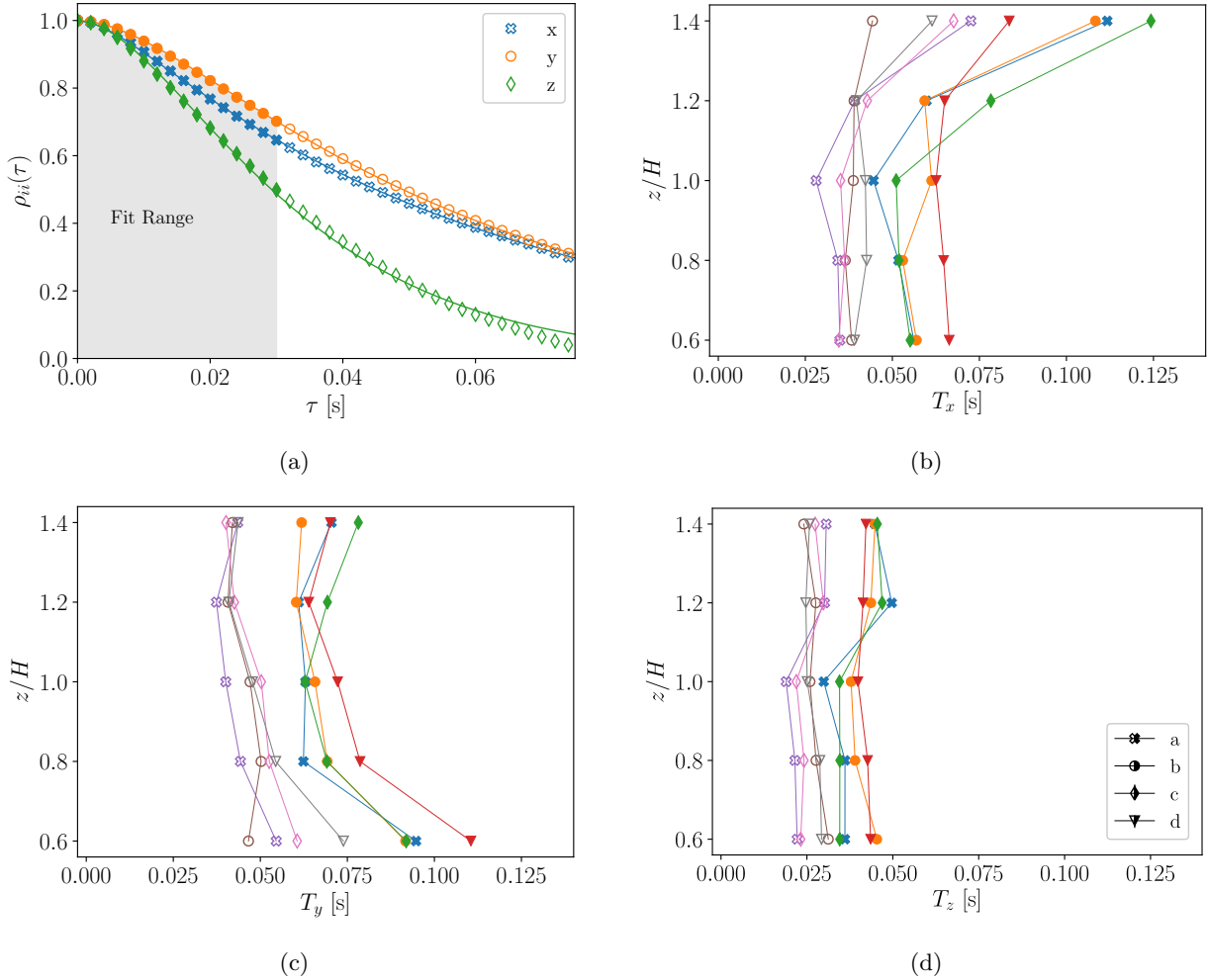


Figure 2: (a) Autocorrelation function of Lagrangian velocity in the sub-volume *b3* and $Re_\infty = 16 \times 10^3$, presented against the time lag, shapes denote data points and lines represent fits to the model Eq. (6). (b)-(d) The Lagrangian timescale for the *x*, *y* and *z* velocity component as a function of sub-volume height. Filled shapes stand for $Re_\infty = 16 \times 10^3$ and empty shapes for $Re_\infty = 26 \times 10^3$.

obtain T_1 and T_2 in each sub-volume and then define $T_i = T_1 + T_2$. It is noted that a calculation of $T_{L,i}$ using the full integral of ρ_{ii} according to the theory, may result in a larger timescale on the order of the turnover timescale for large coherent structures above the canopy. The concave shape of the autocorrelation function at $\tau \rightarrow 0$ implies that the exponential approximation according to first order models, e.g. Eq. (3), is not compatible with our data. Instead, we used the second-order model by Sawford [62], Eq. (6), that does take this concavity into account, similarly to Mordant et al. [74] and Ouellette et al. [41].

We estimated T_i for the three velocity components by fitting the data as shown in Fig. 2(a). The fit range was limited to the time gaps that correspond to a half of the sub-volume crossing time, in order to avoid the possible finite volume effects (as discussed in Appendix C and Ref. [75]). This is a common approach in experimental data analysis because of increased uncertainty of correlations at larger time gaps [76]. Lastly, we note that every data point of ρ_{ii} corresponds to the average of at least 15×10^3 samples, where the relative mean squared error was of the order of a few percents.

The empirical Lagrangian decorrelation times, T_i , are presented in Fig. 2(b,c,d) for each velocity component as a function of height for the two Reynolds numbers tested. Inside the canopy, the values of T_x are roughly constant and increase above the canopy. In contrast, T_y values are highest at the lowest sub-volume yet retain a roughly constant value above the canopy. The values of T_z are the lowest of the three components and show only minor variation with height. Furthermore, the Lagrangian decorrelation times are consistently

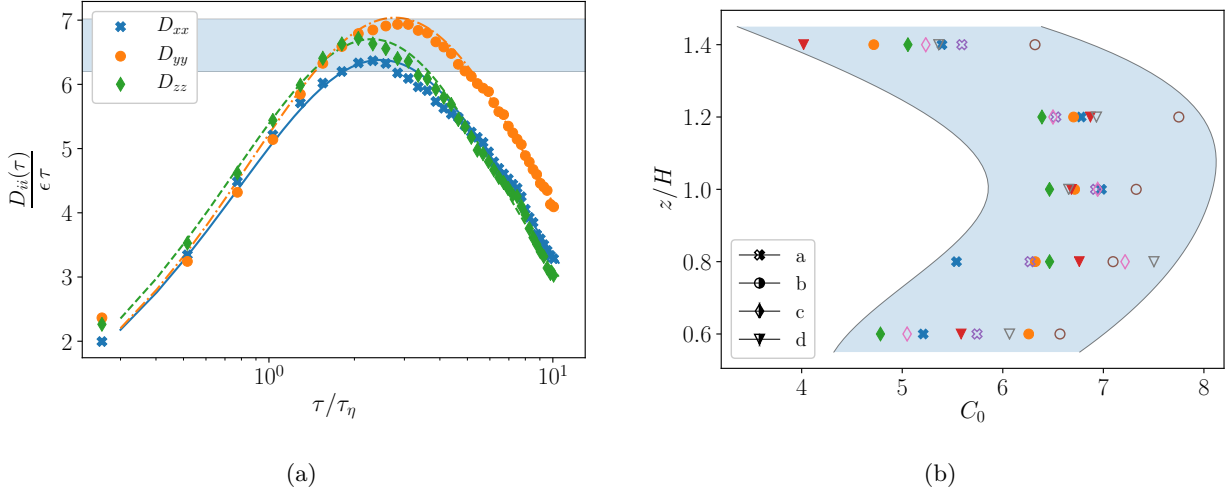


Figure 3: (a) Second order Lagrangian structure function of velocity differences in sub-volume *b3* and $Re = 16 \times 10^3$, presented as a function of time normalized with the inertial-range scaling. The continuous, dashed, and dash-dotted lines represent Sawford’s second order LSM [62] fitted to the x , y and z components respectively. (b) The estimated Kolmogorov constant Eq. (11) from the x velocity component, for all sub-volumes and two Reynolds numbers as a function of height. Full shapes for $Re_\infty = 16 \times 10^3$ and hollow for $Re_\infty = 26 \times 10^3$.

higher for the $Re_\infty = 16 \times 10^3$ case, as compared to the higher $Re_\infty = 26 \times 10^3$ case.

The distributions of T_i can be associated with physical processes that are known to occur in canopy flows. The increase of T_x above the canopy may be related to large scale coherent structures that are known to exist above canopies due to the shear instability, aka the mixing layer analogy [24, 25]. The increase of T_y inside the canopy layer is attributed to the change in the roughness density with height – the lower roughness elements caused an increased frontal area density and increased the “shielding” (e.g. [77]), which contributed to a tunneling effect of a cross-flow inside the canopy layer. Lastly, lower values of T_z as compared to T_x and T_y are in agreement with observations on the Eulerian integral timescales of velocity measurement, for instance by Refs. [33, 50, 78], and may be associated with an inclined orientation of coherent structures that was reported in the literature, e.g. by Shaw et al [78] using two-point Eulerian correlations.

B. Second Order Lagrangian Structure Function

Using the sub-volume averaging, we estimated the Lagrangian second order structure function through its definition, Eq. (4). The results for trajectories in sub-volume *b3* are shown in Fig. 3(a) in a compensated form, $\frac{D_{ii}(\tau)}{\epsilon\tau}$, which corresponds to the Kolmogorov scaling in the inertial range. For high Reynolds number HIT flows, one expects to observe a plateau in the compensated plot. The figure shows that such a plateau does not appear in our data, and instead, only narrow peaks are seen. Such peaks are characteristic of low to moderate Reynolds number flows, and similar observations were reported in numerous previous studies involving other types of flows, Refs. [40, 43, 47, 74, 75, 79–82]. Therefore, we use the typical empirical estimate of $C_{0,i}$, which is defined using the height of the peaks

$$C_{0,i} = \max_{\tau} \left[\frac{D_{ii}(\tau)}{\epsilon\tau} \right]. \quad (11)$$

In the case of sub-volume *b3*, shown in Fig. 3(a), the values obtained are in the range $C_{0,i} \in (6.2, 7.0)$ for the three velocity components, meaning weak anisotropy $\sim \mathcal{O}(10\%)$.

We applied Eq. (11) to the $D_{xx}(\tau)$ obtained in the different sub-volumes in the canopy flow model. The obtained values of $C_{0,x}$ are presented in Fig. 3(b) as a function of height. Values of $C_{0,i}$ calculated with D_{yy}

and D_{zz} were very similar to Fig. 3(b) and are not shown for the sake of brevity. A considerable scatter is seen in the values, roughly $\sim 30\%$, that may be either due horizontal inhomogeneity across sub-volumes through Re_λ variations, or due to a sensitivity of Eq. (11) to small uncertainties in the structure-function. In Fig.3(b), $C_{0,x}$ does not show a dependence on Re_∞ , which is consistent with the behavior of Re_λ . Going from inside the canopy and increasing in z , $C_{0,x}$ initially increases and roughly levels off at $C_{0,x} \approx 6.5$ in the range $1.0 < z \leq 1.2$. Further up above the canopy, $C_{0,x}$ decreased even though Re_λ was seen to be highest at this height level.

The distribution of $C_{0,x}$ with z suggests important conclusions. First, since $C_{0,x}$ is not monotonous with z while Re_λ increases with z in our measurement shows that $C_{0,i}$ is not a function of Re_λ alone in the canopy flow. This is unlike the HIT flows in which C_0 is governed by Re_λ alone (e.g. [81, 83]). Second, the non-monotonous distribution of $C_{0,i}$ can be linked to its empirical definition. In Eq. (11), the empirical estimation of $C_{0,i}$ is sensitive to ϵ , which inherently tie our estimation with the turbulent cascade. Now, while in HIT, ϵ is generally assumed to be constant through the scales, in canopy flows the spectral short-circuiting and the wake-production result in $\epsilon = \epsilon(r) \neq \text{Const.}$ [24]. This process, according to the mechanism suggested by Poggi et al. [33], can lead to an apparent attenuation of C_0 in canopy flows and it has important consequences for modeling dispersion in the environment through LSMs. Thus, through this mechanism, wake-production and short-circuiting can explain the observations in Fig. 3(b).

In Section III A it was observed that the autocorrelation function was concave at the origin (Fig. 2), and that we obtained a good fit for the data using the second-order LSM, Eq. (5). In a homogeneous flow, the Lagrangian structure function and the D_{ii} are simply related by

$$D_{ii}(\tau) = 2\sigma_i^2 [1 - \rho_{ii}(\tau)] . \quad (12)$$

Eq. (12) was used to fit the empirical data for $D_{ii}(\tau)$ where we used the expression for $\rho_{ii}(\tau)$ from the second order LSM, Eq. (6). The fit was performed for the three components of the structure function using a least square algorithm, and the result is shown as lines in Fig. 3(a). The good fits that were obtained for the empirical data show that single-particle statistics in our measurements are captured well by Sawford's second order LSM [62], Eq. (5). This suggests that local homogeneity holds in the short time frame of our measurements, and this will be further examined in Sec. IV B.

IV. LAGRANGIAN RAPID DECORRELATION

To examine the unique feature of the canopy flow, we compare our empirical estimations of T_i with the results of previous studies in homogeneous flows. The comparison allows to highlight the unique features in the canopy flows and to discuss a phenomenology for this case, which includes the turbulence-obstacle interaction.

A. Observation of Rapid Decorrelation in the Canopy Flow

Using the direct empirical estimations of T_i , it is possible to compare with two results of previous investigations that estimated the Lagrangian timescale in the past. In particular, we compare with the ‘‘clean’’, canonical, HIT flows, since this will later aid in establishing a mechanical phenomenology for the canopy flow case.

We first compare the empirical results with the theoretical relation Eq. (4), according to which

$$T_{L,i} = \frac{2v_i'^2}{C_{0,i}\epsilon} . \quad (13)$$

This relation was used previously in LSMs in canopy flows, for example, Refs. [12, 15, 28]. The comparison is shown in Fig. 4(a) through a histogram of the property $T_x / (\frac{2\sigma_u^2}{C_0\epsilon})$, taking values from all the sub-volumes and two Re_∞ . The histogram shows a large scatter of values in the range [0.3–1] with an average of 0.65, and thus implies that the empirically estimated T_i is significantly shorter than the well-known estimation of $T_{L,x}$, Eq. (13).

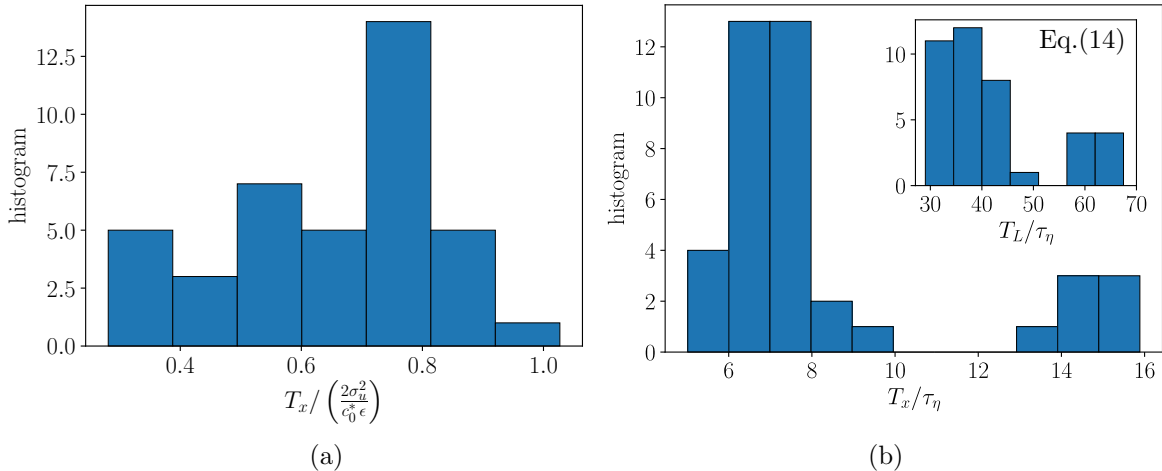


Figure 4: Histograms of Lagrangian de-correlation times in the x direction from all sub-volumes and two Re_∞ , normalized with the (a) large scale diffusivity matching and (b) the dissipation timescale.

The second comparison, in Fig. 4(b), compares the separation of scales in our canopy flow with that of HIT at similar Re_λ . A histogram of the decorrelation times, T_x , normalized with the dissipation timescale, τ_η , is shown in Fig. 4(b). The results fall into two groups with values of the order $T_x \sim 5 - 10\tau_\eta$, and $T_x \sim 13 - 16\tau_\eta$ that were seen to occur at different height levels, consistent with the increase of Re_λ farther away from the wall. Given the moderate – high range of Re_λ in our experiment, the separation T_x/τ_η is low when compared to values of T_L/τ_η usually encountered in HIT at comparable Re_λ . For example, Sawford et al. [84] suggested

$$\frac{T_L}{\tau_\eta} = \left[4.77 + \left(\frac{Re_\lambda}{12.6} \right)^{4/3} \right]^{3/4} \quad (14)$$

following the empirical fit to DNS data. Using the Re_λ values from our measurements, the estimates using Eq. (14) are plotted in the inset of Fig. 4(b), where the values are seen to be roughly an order of magnitude higher than those obtained by directly fitting the autocorrelation functions. Therefore, Fig. 4 suggests that the separation of scales in our canopy flow is much lower than what is expected in the comparable HIT case.

In Fig. 4, T_i was compared with properties estimated using spatial information of the flow, namely ϵ . Therefore, we can reinforce the above observation of relatively small separation of scales using a Lagrangian property that characterizes the small scales – the particles' acceleration, $\mathbf{a} = \frac{d\mathbf{v}}{dt}$. Specifically, we contrast the autocorrelation of v_i and a_i in our canopy flow with those in a comparable HIT flow. For the HIT flow, we use the DNS data available from the Johns Hopkins Turbulence Database (JHTDB) [82, 85]. We downloaded this benchmark dataset for the previous study in Ref. [53], and we use it here again to compare the autocorrelation functions. Autocorrelation functions from the DNS data and the data from sub-volume b3 are plotted together in Fig. 5. Note that the Re_λ in both cases are very similar, $Re_\lambda \approx 440$ in sub-volume b3 and $Re_\lambda \approx 433$ in the DNS [82], and so they should present similar separation of scales if $T_L/\tau_\eta = f(Re_\lambda)$ alone. Fig. 5 shows that autocorrelation of the acceleration components decay at rates very similar to each other in both cases. However, the velocity in the canopy flow decorrelates much faster than in the HIT case. To be more quantitative, denoting by T_a the time of the first zero crossing of the acceleration, it was found that $T_x/T_a \approx 4.7$ for the canopy data, while $T_x/T_a \approx 13.5$ for the HIT case. Therefore, Fig. 5 shows that while the T_a was roughly the same in both cases, the velocity, which is a larger scale property, became decorrelated roughly 3 times faster in the canopy flow as compared to the HIT counterpart. This observation reinforces that the separation of timescales in our flow is lower than in the comparable HIT case.

Inclusively, Figs. 4 and 5 demonstrate that the Lagrangian velocity components in our canopy flow became decorrelated much faster than what would be expected in homogeneous, isotropic turbulent flows at similar Reynolds numbers. In particular, the above demonstrated that in the canopy flows, unlike the HIT case, T_i/τ_η

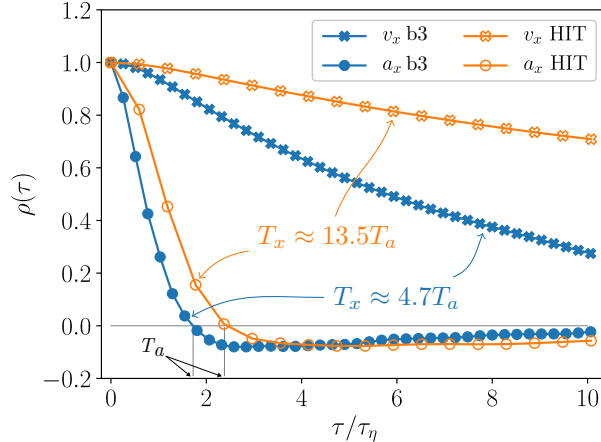


Figure 5: Lagrangian auto correlation functions of the acceleration component and the velocity component of Lagrangian particles. Hollow symbols correspond to trajectories for the DNS [53, 82, 85] and filled symbols to canopy trajectories from sub-volume b3 at $Re_\infty = 16 \times 10^3$.

is *not* a function of the Reynolds number alone. This observation will be termed here *rapid decorrelation*. In the following section we shall examine the main cause of the rapid decorrelation, and in particular, we consider two possible hypothesis: i) the rapid decorrelation was due to the flow inhomogeneity, and ii) that it was due to the wake-production.

B. The Influence of Inhomogeneity on the Velocity Decorrelation

Let us examine the hypothesis that the rapid decorrelation was caused by the flow inhomogeneity. Thomson [19] noted that in inhomogeneous flows “ T_i is not the integral timescale but simply a (rather loosely defined) *local decorrelation* timescale”. This could have important consequences for dispersion modeling with LSMs. For example, considering the first order LSMs, in the inhomogeneous flows, the equations are different from the Langevin equation Eq. (3). In particular, α_i should depend on the Eulerian flow parameters, namely the gradients of $\langle \mathbf{u} \rangle$, in a complex and non-unique way (as was discussed in the introduction, Section I).

We first compare the calculated values T_i with a timescale at which we expect the inhomogeneity to become dominant. In our experiment, the turbulent intensity is very high – well above 100% inside the canopy layer; therefore, the RMS of the velocity, $v' = (\sum_i \langle v_i'^2 \rangle)^{1/2}$, and not the average, is a proper convection velocity scale (since $v' > \langle v_i \rangle$ this choice is also more conservative). In addition, the length scale at which inhomogeneity is felt in the canopy flow is comparable to the size of the roughness obstacles, namely $\sim H$. Thus, the timescale appropriate for inhomogeneity to affect the particles in our flow is H/v' . For all the sub-volumes in the dataset, we estimated the fraction $\frac{H/v'}{T_x}$, which gave values in the range 2.5–6. Therefore, the expected time for particles to be affected by the inhomogeneity was much longer than typical times of decorrelation. This suggests that by the time Lagrangian particles could be affected by the inhomogeneity, their velocity had become decorrelated. The conclusion is that inhomogeneity was probably not the main cause for the rapid decorrelation.

The effects of inhomogeneity on our measurements could be more rigorously quantified by analyzing the changes of the average particle kinetic energy by following Novikov [86]. In particular, using the OU representation, we multiply Eq. (1) by v_i , and obtain a stochastic model for the particles’ kinetic energy. Then, denoting the random impulse as $\beta_i d\xi_i \equiv f_i dt$, where $f_i (\equiv a_i - v_i^2/T_i)$ is a random force component, and taking the average, we obtain an equation for the average rate of change of the particle kinetic energy

$$\frac{1}{2} \left\langle \frac{d(v_i^2)}{dt} \right\rangle = \left\langle -\frac{v_i^2}{T_i} \right\rangle + \langle v_i f_i \rangle. \quad (15)$$

The term $\langle -\frac{v_i^2}{T_i} \rangle$ is negative, and thus a loss term that we denote as $\epsilon^* \equiv \langle \frac{v_i^2}{T_i} \rangle$. On the other hand, $\langle v_i f_i \rangle$

is an average power, and is thus a gain term that we denote $\mathcal{P}^* \equiv \langle v_i f_i \rangle$. In a statistical steady state the right-hand-side of Eq. (15) is equal to zero, so there is an equilibrium of the loss and gain terms –

$$\epsilon_i^* = \mathcal{P}^* . \quad (16)$$

Since in inhomogeneous flows Lagrangian statistics are non-stationary, the equilibrium condition, Eq. (16), can be used to probe departures from the homogeneous state. Thus, using the definitions of f_i , ϵ^* and \mathcal{P}^* , we estimated the ratio \mathcal{P}^*/ϵ^* and compared it to the homogeneous value 1. The results are shown through a histogram in Fig. 6(a) that counts the number of sub-volumes with particular values of \mathcal{P}^*/ϵ^* . The Figure shows that for most of the sub-volumes (34 out of 40) the ratio lies within 10% of 1, namely that for the great majority of cases local homogeneity is a good approximation. The figure also shows that for certain cases the deviation from equilibrium was higher - up to 30%. These cases occurred for the higher Re_∞ and mostly at the top of the canopy layer where the mean velocity shear is typically the highest. Therefore, Fig. 6 shows that the effect of inhomogeneity on our measurements of Lagrangian statistics was generally small in comparison the rates of gain and loss of kinetic energy of individual particles. In particular, we find that the observed deviations from equilibrium of $\sim 10\%$ are too small to explain rapid decorrelation, since the separation of scales T_i/τ_η in our measurements was roughly five times lower than what is expected in HIT.

To further demonstrate the above argument of near local homogeneity we calculated conditional statistics. We divided the particles in sub-volume b3 into two groups: *ascending particles*, that left the sub-volume further away from the bottom wall than where they entered it, and *descending particles* that went the opposite way and approached the wall. Fig. 6(b) shows the velocity autocorrelation for the ascending/descending groups; both are seen to decay at roughly the same rate as the autocorrelations of the rest of particles. Namely, the influence of conditional statistics on the autocorrelation is too small to explain the drastically smaller T_i values observed above. Thus, Fig. 6 too suggests on a sub-leading role of inhomogeneity in causing the rapid decorrelation.

To conclude, the above analyses indicate that the rapid decorrelation of the velocity did not occur due to inhomogeneity. This was deduced from the value of $\frac{H/v'}{T_i}$, from the steady state condition Eq. (16), and through conditional statistics.

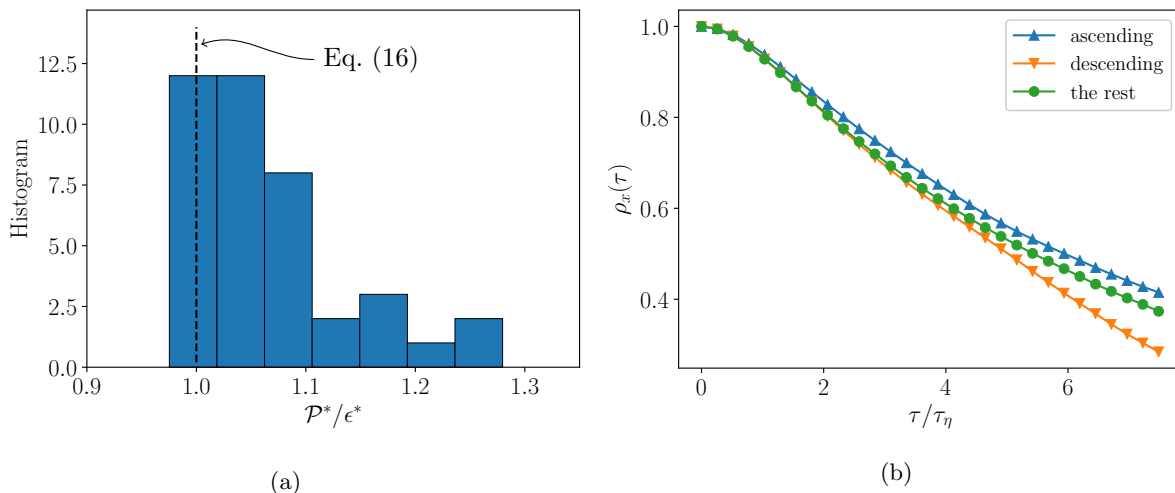


Figure 6: (a) A histogram, showing the number of sub-volumes with particular values of the ratio between gain and loss of particle kinetic energy. (b) Autocorrelation function of particles in sub-volume $b3$ and $Re_\infty = 16 \times 10^3$, conditioned on the ascending / descending / neither state of particles.

C. Turbulence–Obstacle Interaction as the Source for Rapid Decorrelation

Next we examine the hypothesis that the rapid decorrelation was the consequence of wake-production due to direct interaction of the flow with the canopy obstacles that short-circuits the energy cascade [24]. This hypothesis is supported by the observation that C_0 was altered by the wake-production in accordance with the arguments of Poggi et al. [33]. Specifically, it demonstrates that wake-production can indeed influence Lagrangian statistics, and in particular, cause a reduction of T_i through Eq. (13).

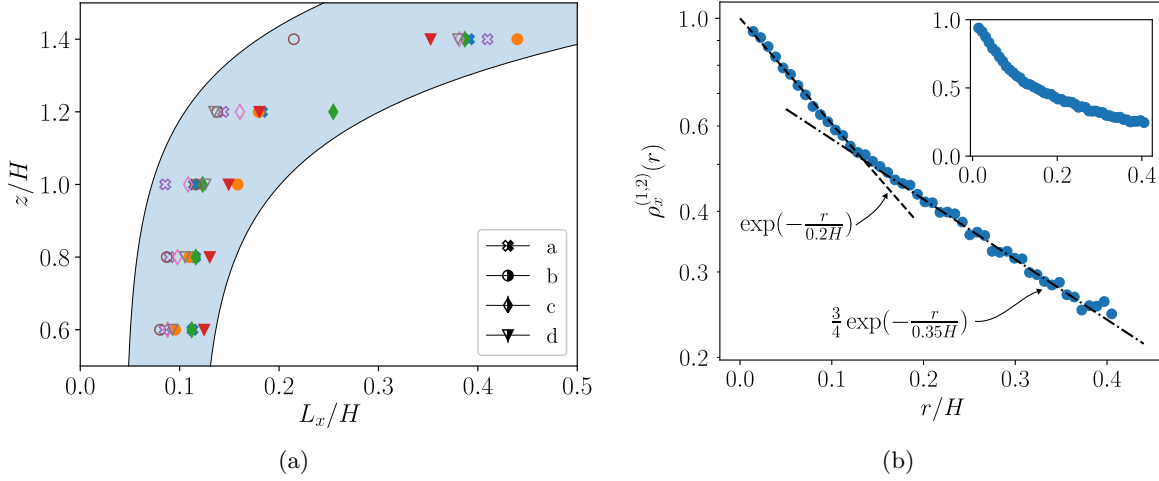


Figure 7: (a) Lagrangian dispersion length scale $L_x = T_x \sigma_x$, presented as a function of height, both axes normalized by H . (b) Two-particle spatial correlation function, plotted against distance normalized by the canopy top height. Data for particles in sub-volume b3.

The wake production causes a direct transfer of turbulent kinetic energy to flow scales with sizes that are determined by the geometry of the roughness obstacles [24, 87]. Therefore, if the hypothesis was true we would expect the dispersion in this wake regime to be dominated by flow disturbances with a similar size. The appropriate length scale of dispersion is $L_i = \sigma_i T_{L,i}$, which was observed to be correlated with the scale of forcing in previous experiments (Refs. [74, 88]). The width of our obstacles was $d = 0.04H$, so if the hypothesis is true we should see $L_i \sim d$. The $L_x = T_x \sigma_x$ was estimated in the different sub-volumes and is presented in Fig. 7(a) versus the height. Inside the canopy layer, $z \leq H$, the L_x is nearly constant, $L_x \approx 0.1H = 2.5d$ independently of Re_∞ , which may well be due to such wake disturbances. Above the layer, L_x increases, reaching $\approx 0.35H$ at the highest sub-volume. The increase of L_x at $z > H$ is consistent with the notion of weakening of the wake's influence above the canopy. Therefore, the estimated values of L_x are consistent with the hypothesis that rapid decorrelation occurred due to the flow disturbances in the obstacles' wakes.

To support the argument that some disturbances occur in our flow at the scale L_x , we examine the two-particle spatial correlation function. Specifically, let us define

$$\rho_i^{(1,2)}(r) = \frac{\langle v_i^{(1)}(t) v_i^{(2)}(t) | r(t) \rangle}{\text{Var}[v_i'(t)]_r} \quad (17)$$

where $v_i^{(1)}$ and $v_i^{(2)}$ are the fluctuation (around the sub-volume mean, $\mathbf{v}' = \mathbf{v} - \langle \mathbf{u} \rangle$) of the velocity component of two different particles at the same time, and where the average in the numerator is performed for pairs of trajectories with a distance of $r(t) = |\mathbf{x}^{(1)}(t) - \mathbf{x}^{(2)}(t)|$ between them. In the denominator, $\text{Var}[v_i'(t)]_r$ is the variance of the velocity components calculated over the same ensemble of particles used in the numerator. Note that $\rho_i^{(1,2)}$ is a correlation with no separation in time but only in space, and thus can be used to examine the spatial structure of the flow. The definition Eq. (17) is analogous to the Eulerian two-point spatial velocity correlation function that is often performed using a static and a moving probe (for instance by Shaw et al. [78]), however, $\rho_i^{(1,2)}(r)$ is isotropic by construction since the average is performed over spherical

shells.

The two-particle correlation of v'_x , calculated using trajectories from sub-volume b3, is shown in Fig. 7(b). The same data is shown in linear-log scales in the main figure and in linear scales in the inset. The $\rho_i^{(1,2)}(r)$ decreases monotonously with r . In the range $r \lesssim 0.12H$, the correlation decreases faster than at $r \gtrsim 0.12H$. In the linear-log scales, the data at each interval roughly fits a straight line, where in each interval it has a different slope. Therefore, the data points were fitted exponential decays with a different rate in each of these two ranges of r , which provided a good approximations of the data. The two fits, shown in dashed and dot-dashed lines, highlight the transition of the $\rho_i^{(1,2)}(r)$ from one rate of decay to another at $r \approx 0.12H$. The scale of transition is nearly equal to the dispersion length scale in this sub-volume – $L_x \approx 0.12H$ (see Fig. 17 at $z = H$). Since the velocity at two-points becomes decorrelated faster for $r < L_x$ than for $r > L_x$, the observed transition of the $\rho_i^{(1,2)}(r)$ from one rate of decay to another supports the argument of an existence of flow disturbances at this scale. Furthermore, an existence of such flow disturbances at $L_x = \sigma_x T_x \sim d$, supports the argument that rapid decorrelation in our flow occurred due to small-scale disturbances in the obstacle’s wakes.

In light of what was presented above, we understand that wake production is the main cause of the rapid decorrelation of Lagrangian velocity, with the effect being stronger than the one of the inhomogeneity. The important conclusion is that in the canopy flow T_i/τ_η is not $f(Re_\lambda)$ alone, which is different from the HIT case. This was demonstrated through the change of the dispersion length scale with the height and by examining the two particle correlation. This is by no means a conclusive proof and requires further study, using a flow with various degrees of spectral short-circuiting versus inhomogeneity. Such a study is out of the scope of this work.

V. DISCUSSION & CONCLUSIONS

In this work, we used experimental measurements to make direct estimations of Lagrangian statistics in a wind-tunnel canopy flow model with applications to LSMs. We found that turbulence-obstacle interaction, through wake-production and spectral short-circuiting, had strong impact on the Lagrangian second-order structure function and velocity autocorrelation in our experiment. In particular, we observed that the value of C_0 was altered in our canopy flow, which is in accordance with the conclusions of Poggi et al. [33]. In addition, the decorrelation timescale of the Lagrangian velocity was much shorter than would have been expected in comparable homogeneous flows. The important conclusion is that in the canopy flows, neither C_0 nor T_i are functions only of Re_λ , which is unlike the homogeneous flows.

Due to the rapid decorrelation, the separation of scales T_i/τ_η was small in our flow. Namely, the spectral short-circuiting in our canopy flow caused significant finite Reynolds number effects to appear in Lagrangian statistics although Re_λ was in the range of 350–850. Accordingly, our empirical Lagrangian autocorrelation was seen to fit very well to the second order model Eq. (5). Essentially, this is a demonstration that finite Reynolds number effects can be important in cases where the Richardson-Kolmogorov cascade is short circuited.

An important observation was that the Lagrangian particle velocity became decorrelated before the particles had the opportunity to “feel” the inhomogeneity of the canopy flow. Namely, our results, and in particular the analysis of particle kinetic energy in Sec. IV B, show that local isotropy and homogeneity provides a good approximation for small scale Lagrangian statistics. This supports the applicability of the localized near field theory [6] to dispersion modeling in dense canopies.

To conclude, the observations presented in this work make up a unique view on the Lagrangian dynamics in the canopy flows in the small scales. It is our view that short term dispersion modeling in canopy flows through LSMs may achieve increased accuracy in utilizing the principle of rapid decorrelations in the dense canopies that are governed by wake dynamics. This also highlights the importance of Lagrangian statistics gathered directly in the Lagrangian framework. Other topics that were not dealt with here concern the effect of mechanical diffusion, the mixing-layer analogy, and the inhomogeneity, that due to our small scale of observation could not have been assessed here, and thus leave considerable scope for future investigations.

ACKNOWLEDGMENT

The authors are grateful to Meni Kohn, Sabrina Shlain, Gregory Gulitski, Valery Babin, Amos Shick and Mordechai Hotovely, for their assistance in preparing and performing the wind tunnel experiment. This study is supported by the PAZY grant number 2403170.

-
- [1] R. E. Britter and S. R. Hanna. Flow and dispersion in urban areas. *Annual Reviews in Fluid Mechanics*, 35:469–496, 2003.
 - [2] R. Nathan, G. G. Katul, H. S. Horn, S. M. Thomas, R. Oren, R. Avissar, S. W. Pacala, and S. A. Levin. Mechanisms of long-distance dispersal of seeds by wind. *Nature*, 418, 2002.
 - [3] M. R. Raupach and A. S. Thom. Turbulence in and above plant canopies. *Annual Review of Fluid Mechanics*, 13(1):97–129, 1981.
 - [4] M. R. Raupach. A lagrangian analysis of scalar transfer in vegetation canopies. *Quarterly Journal of the Royal Meteorological Society*, 113(107-120), 1987.
 - [5] E. Gavze and E. Fattal. Description of a turbulent cascade by a Fokker-Planck equation. *Boundary Layer Meteorology*, 169:297–326, 2018.
 - [6] M. R. Raupach. Applying lagrangian fluid mechanics to infer scalar source distributions from concentration profiles in plant canopies. *Agricultural and Forest Meteorology*, 47:85–108, 1989.
 - [7] T. K. Flesch and J. D. Wilson. A two-dimensional trajectory-simulation model for non-gaussian, inhomogeneous turbulence within plant canopies. *Boundary Layer Meteorology*, 61:349–374, 1992.
 - [8] J.D. Wilson and B.L. Sawford. Review of lagrangian stochastic models for trajectories in the turbulent atmosphere. *Boundary-Layer Meteorology*, 78:191–210, 1996.
 - [9] M. W. Rotach, S.-E. Gryning, and C. Tassone. A two-dimensional lagrangian stochastic dispersion model for daytime conditions. *Quarterly Journal of the Royal Meteorological Society*, 122(530):367–389, 1996.
 - [10] D. Baldocchi. Flux footprints within and over forest canopies. *Boundary-Layer Meteorology*, 85(2):273–292, Nov 1997.
 - [11] R. Leuning, O. T. Denmead, A. Miyata, and J. Kim. Source/sink distributions of heat, water vapour, carbon dioxide and methane in a rice canopy estimated using lagrangian dispersion analysis. *Agricultural and Forest Meteorology*, 104:233–249, 2000.
 - [12] D. E. Aylor and T. K. Flesch. Estimating spore release rates using a lagrangian stochastic simulation model. *Journal of Applied Meteorology*, 40(7):1196–1208, 2001.
 - [13] R. W. Arritt, C. A. Clark, A. S. Goggi, H. Lopez Sanchez, M. E. Westgate, and J. M. Riese. Lagrangian numerical simulations of canopy air flow effects on maize pollen dispersal. *Field Crops Research*, 102(2):151 – 162, 2007.
 - [14] Gleicher S. C., Chamecki M., Isard S. A., Pan Y., and Katul G. G. Interpreting three-dimensional spore concentration measurements and escape fraction in a crop canopy using a coupled eulerian–lagrangian stochastic model. *Agricultural and Forest Meteorology*, 194:118 – 131, 2014.
 - [15] T. Duman, A. Trakhtenbrot, D. Poggi, M. Cassiani, and G. G. Katul. Dissipation intermittency increases long-distance dispersal of heavy particles in the canopy sublayer. *Boundary-Layer Meteorology*, 159(1):41–68, Apr 2016.
 - [16] E. Fattal, O. Buchman, and E. Gavze. A lagrangian-stochastic model for pollutant dispersion in the urban boundary layer over complex terrain - comparison with haifa campaigns. *23rd Symposium on Boundary Layers and Turbulence, American Meteorological Society*, 8A.4, 2018.
 - [17] M. Obukhov, A. Description of turbulence in terms of lagrangian variables. volume 6 of *Advances in Geophysics*, pages 113–116. Elsevier, 1959.
 - [18] R. Friedrich and J. Peinke. Description of a turbulent cascade by a Fokker-Planck equation. *Phys. Rev. Lett.*, 78:863–866, 1997.
 - [19] D. J. Thomson. Criteria for the selection of stochastic models of particle trajectories in turbulent flows. *Journal of Fluid Mechanics*, 180:529–556, 1987.
 - [20] M. S. Borgas and B. L. Sawford. Stochastic equations with multifractal random increments for modeling turbulent dispersion. *Physics of Fluids*, 6(2):618–633, 1994.
 - [21] A. M. Reynolds. On the dynamical content of Lagrangian stochastic models in the well-mixed class. *Boundary-Layer Meteorology*, 103(May 2001):143–162, 2002.
 - [22] J. D. Wilson and T. K. Flesch. Trajectory curvature as a selection criterion for valid Lagrangian stochastic dispersion models. *Bound.-Layer Meteorol.*, 84(2):411–425, 1997.
 - [23] B. L. Sawford. Rotation of trajectories in lagrangian stochastic models of turbulent dispersion. *Bound.-Layer Meteorol.*, 93:411–424, 1999.
 - [24] J. Finnigan. Turbulence in plant canopies. *Annual Review of Fluid Mechanics*, 32:519–571, 2000.

- [25] M. R. Raupach, J. J. Finnigan, and Y. Brunet. Coherent eddies and turbulence in vegetative canopies: The mixing-layer analogy. *Boundary-Layer Meteorology*, 78:351–382, 1996.
- [26] R. H. Shaw and I. Seginer. Calculation of velocity skewness in real and artificial plant canopies. *Boundary Layer Meteorology*, 39:315–332, 1987.
- [27] H. M. Nepf. Drag, turbulence, and diffusion in flow through emergent vegetation. *Water Resources Research*, 35(2), 1999.
- [28] D. Poggi, G. Katul, and J. Albertson. Scalar dispersion within a model canopy: Measurements and three-dimensional lagrangian models. *Advances in Water Resources*, 29(2):326 – 335, 2006. Experimental Hydrology: A Bright Future.
- [29] T. Duman, G. G. Katul, M. B. Siqueira, and M. Cassiani. A velocity–dissipation lagrangian stochastic model for turbulent dispersion in atmospheric boundary-layer and canopy flows. *Boundary-Layer Meteorology*, 152(1):1–18, Jul 2014.
- [30] A. M. Reynolds. On the formulation of lagrangian stochastic models of scalar dispersion within plant canopies. *Boundary-Layer Meteorology*, 86(2):333–344, Feb 1998.
- [31] Ü Rannik, M. Aubinet, O. Kurbanmuradov, K. K. Sabelfeld, T. Markkanen, and T. Vesala. Footprint analysis for measurements over a heterogeneous forest. *Boundary-Layer Meteorology*, 97(1):137–166, Oct 2000.
- [32] W. J. Massman and J. C. Weil. An analytical one-dimensional second-order closure model for turbulence statistics and the lagrangian time scale within and above plant canopies of arbitrary structure. *Boundary-Layer Meteorology*, 91:81–107, 1999.
- [33] D. Poggi, G. G. Katul, and M. Cassiani. On the anomalous behavior of the lagrangian structure function similarity constant inside dense canopies. *Atmospheric Environments*, 2008.
- [34] S. B. Pope and Y. L. Chen. The velocity-dissipation probability density function model for turbulent flows. *Physics of Fluids A: Fluid Dynamics*, 2(8):1437–1449, 1990.
- [35] G. A. Voth, K. Satyanarayan, and E. Bodenschatz. Lagrangian acceleration measurements at large reynolds numbers. *Physics of Fluids*, 10(9):2268, 1998.
- [36] S. Ott and J. Mann. An experimental investigation of the relative diffusion of particle pairs in three-dimensional turbulent flow. *Journal of Fluid Mechanics*, 422:207–223, 2000.
- [37] N. Mordant, J. Delour, E. Léveque, A. Arnéodo, and J.-F. Pinton. Long time correlations in lagrangian dynamics: A key to intermittency in turbulence. *Phys. Rev. Lett.*, 89:254502, Dec 2002.
- [38] L. Biferale, G. Boffetta, A. Celani, B. J. Devenish, A. Lanotte, and F. Toschi. Lagrangian statistics of particle pairs in homogeneous isotropic turbulence. *Physics of Fluids*, 17, 2005.
- [39] M. Bourgoin, N. T. Ouellette, H. Xu, J. Berg, and E. Bodenschatz. The role of pair dispersion in turbulent flow. *Science*, 311:835–838, 2006.
- [40] P. K. Yeung, S. B. Pope, and B. L. Sawford. Reynolds number dependence of lagrangian statistics in large numerical simulations of isotropic turbulence. *Journal of Turbulence*, 7:N58, 2006.
- [41] N. Ouellette, H. Xu, M. Bourgoin, and E. Bodenschatz. Small-scale anisotropy in lagrangian turbulence. *New Journal of Physics*, 8, 2006.
- [42] J. Berg, B. Lüthi, J. Mann, and S. Ott. Backwards and forwards relative dispersion in turbulent flow: an experimental investigation. *Physical Review E*, 74, 2006.
- [43] J. Bec, L. Biferale, M. Cencini, A. S. Lanotte, and F. Toschi. Effects of vortex filaments on the velocity of tracers and heavy particles in turbulence. *Physics of Fluids*, 18(8):081702, 2006.
- [44] M. Guala, A. Liberzon, A. Tsinober, and W. Kinzelbach. An experimental investigation on lagrangian correlations of small-scale turbulence at low Reynolds number. *Journal of Fluid Mechanics*, 574:405–427, 2007.
- [45] R. J. E. Walpot, C. W. M. van der Geld, and J. G. M. Kuerten. Determination of the coefficients of langevin models for inhomogeneous turbulent flows by three-dimensional particle tracking velocimetry and direct numerical simulation. *Physics of Fluids*, 19, 2007.
- [46] A. Arnéodo, R. Benzi, J. Berg, L. Biferale, E. Bodenschatz, A. Busse, E. Calzavarini, B. Castaing, M. Cencini, L. Chevillard, R. T. Fisher, R. Grauer, H. Homann, D. Lamb, A. S. Lanotte, E. Léveque, B. Lüthi, J. Mann, N. Mordant, W.-C. Müller, S. Ott, N. T. Ouellette, J.-F. Pinton, S. B. Pope, S. G. Roux, F. Toschi, H. Xu, and P. K. Yeung. Universal intermittent properties of particle trajectories in highly turbulent flows. *Phys. Rev. Lett.*, 100:254504, Jun 2008.
- [47] F. Toschi and E. Bodenschatz. Lagrangian properties of particles in turbulence. *Annual Review of Fluid Mechanics*, 41(1):375 – 404, 2009.
- [48] Alex Liberzon, Beat Lüthi, Markus Holzner, Søren Ott, Jacob Berg, and Jakob Mann. On the structure of acceleration in turbulence. *Physica D: Nonlinear Phenomena*, 241(3):208 – 215, 2012. Special Issue on Small Scale Turbulence.
- [49] R. Scatamacchia, L. Biferale, and F. Toschi. Extreme events in the dispersions of two neighboring particles under the influence of fluid turbulence. *Phys. Rev. Lett.*, 109:144501, Oct 2012.
- [50] A. Di Bernardino, P. Monti, G. Leuzzi, and G. Querzoli. Water-channel estimation of eulerian and lagrangian time scales of the turbulence in idealized two-dimensional urban canopies. *Boundary-Layer Meteorology*, 2017.
- [51] N. Stelzenmüller, J. I. Polanco, L. Vignal, I. Vinkovic, and N. Mordant. Lagrangian acceleration statistics in a turbulent channel flow. *Physical Review Fluids*, 2:054602, May 2017.

- [52] J.I. Polanco, I. Vinkovic, N. Stelzenmuller, N. Mordant, and M. Bourgoïn. Relative dispersion of particle pairs in turbulent channel flow. *International Journal of Heat and Fluid Flow*, 71:231 – 245, 2018.
- [53] Ron Shnapp and Alex Liberzon. Generalization of turbulent pair dispersion to large initial separations. *Phys. Rev. Lett.*, 120:244502, Jun 2018.
- [54] A. Celani, M. Cencini, M. Vergassola, E. Villermaux, and D. Vincenzi. Shear effects on passive scalar spectra. *Journal of Fluid Mechanics*, 523:99108, 2005.
- [55] E. Pitton, C. Marchioli, V. Lavezzo, A. Soldati, and F. Toschi. Anisotropy in pair dispersion of inertial particles in turbulent channel flow. *Physics of Fluids*, 24(7):073305, 2012.
- [56] R. Shnapp, E. Shapira, D. Peri, Y. Bohbot-Raviv, E. Fattal, and A. Liberzon. Extended 3D-PTV for direct measurements of Lagrangian statistics of canopy turbulence in a wind tunnel. *Scientific Reports*, 9(7405), 2019.
- [57] Y. Bohbot-Raviv, R. Shnapp, A. Liberzon, V. Babin, M. Hotoveli, A. Shick, and E. Fattal. Turbulence statistics of canopy-flows using novel lagrangian measurements within an environmental wind tunnel. *Physmod, LHEEA-DAUC, Ecole Centrale de Nantes*, 2017.
- [58] S. B. Pope. *Turbulent Flows*. Cambridge University Press, 2000.
- [59] C. W. Gardiner. *Handbook of Stochastic Methods for Physics, Chemistry and the Natural Sciences*, 1997.
- [60] J. L. Doob. The brownian movement and stochastic equations. *Annals of Mathematics*, 43(2):351–369, 1942.
- [61] A. S. Monin and A. M. Yaglom. *Statistical Fluid Mechanics*. Dover Publications inc., 1972.
- [62] B. L. Sawford. Reynolds number effects in lagrangian stochastic models of turbulent dispersion. *Physics of Fluids A: Fluid Dynamics*, 3:1577, 1991.
- [63] S. Du, B. L. Sawford, J. D. Wilson, and D. J. Wilson. Estimation of the kolmogorov constant (c_0) for the lagrangian structure function, using a secondorder lagrangian model of grid turbulence. *Physics of Fluids*, 7(12):3083–3090, 1995.
- [64] A. M. Reynolds. A second-order lagrangian stochastic model for particle trajectories in inhomogeneous turbulence. *Quarterly Journal of the Royal Meteorological Society*, 125:557, 1999.
- [65] Th. Dracos. *Three-Dimensional Velocity and Vorticity Measuring and Image Analysis Technique: Lecture Notes from the short course held in Zurich, Switzerland*. Kluwer Academic Publisher, 1996.
- [66] OpenPTV consortium. Open source particle tracking velocimetry, 2014.
- [67] Y. Meller and A. Liberzon. Particle data management software for 3dparticle tracking velocimetry and related applications – the flowtracks package. *Journal of Open Research Software*, 2016.
- [68] R. Shnapp. Wind tunel canopy flow 3d-ptv. YouTube, 2018. <https://www.youtube.com/watch?v=NMPcWiWUqRY>.
- [69] A. N. Kolmogorov. The local structure of turbulence in incompressible viscous fluid for very large reynolds numbers. *Cr Acad. Sci. URSS*, 30:301–305, 1941.
- [70] K. R. Sreenivasan. On the universality of the kolmogorov constant. *Physics of Fluids*, 7:2778 – 2784, 1995.
- [71] M. Chamecki and N. L. Dias. The local isotropy hypothesis and the turbulent kinetic energy dissipation rate in the atmospheric surface layer. *Quart. J. Roy. Meteor. Soc.*, 130:2733–2752, 2004.
- [72] D. Poggi and G. G. Katul. Evaluation of the turbulent kinetic energy dissipation rate inside canopies by zero- and level-crossing density methods. *Boundary-Layer Meteorology*, 136(2):219–233, Aug 2010.
- [73] H. Tennekes and J. L. Lumley. *A First Course in Turbulence*. The MIT Press, 1972.
- [74] N. Mordant, E. L ev eque, and J.-F. Pinton. Experimental and numerical study of the lagrangian dynamics of high reynolds turbulence. *New Journal of Physics*, 6(116), 2004.
- [75] L. Biferale, E. Bodenschatz, M. Cencini, A. S. Lanotte, N. T. Ouellette, F. Toschi, and H. Xu. Lagrangian structure functions in turbulence: A quantitative comparison between experiment and direct numerical simulation. *Physics of Fluids*, 20(6):065103, 2008.
- [76] W.K. George, P.D. Beuther, and J.L. Lumley. Processing of random signals. In *Proceedings of the Dynamic Flow Conference 1978 on Dynamic Measurements in Unsteady Flows*. Springer, Dordrecht, 1978.
- [77] C. Vanderwel and B. Ganapathisubramani. Turbulent boundary layers over multiscale rough patches. *Boundary-Layer Meteorology*, 172(1):1–16, Jul 2019.
- [78] R. H. Shaw, Y. Brunet, J. J. Finnigan, and M. R. Raupach. A wind tunnel study of air flow in waving wheat: Two-point velocity statistics. *Boundary-Layer Meteorology*, 76(4):349–376, Dec 1995.
- [79] P. K. Yeung and S. B. Pope. Lagrangian statistics from direct numerical simulations of isotropic turbulence. *Journal of Fluid Mechanics*, 207:531–586, 1989.
- [80] N. Mordant, P. Metz, O. Michel, and J.F. Pinton. Measurement of lagrangian velocity in fully developed turbulence. *Physical Review Letters*, 87, 2001.
- [81] B. L. Sawford and P. K. Yeung. Kolmogorov similarity scaling for one-particle lagrangian statistics. *Physics of Fluids*, 23(9):091704, 2011.
- [82] H. Yu, K. Kanov, E. Perlman, J. Graham, E. Frederix, R. Burns, A. Szalay, G. Eyink, and C. Meneveau. Studying lagrangian dynamics of turbulence using on-demand fluid particle tracking in a public turbulence database. *Journal of Turbulence*, 2012.
- [83] R.-C. Lien and E. A. DAsaro. The kolmogorov constant for the lagrangian velocity spectrum and structure function. *Physics of Fluids*, 14(12):4456–4459, 2002.
- [84] B. L. Sawford, P. K. Yeung, and J. F. Hackl. Reynolds number dependence of relative dispersion statistics in isotropic turbulence. *Physics of Fluids*, 20(6):065111, 2008.

- [85] Y. Li, E. Perlman, M. Wan, Y. Yang, R. Burns, C. Meneveau, R. Burns, S. Chen, A. Szalay, and G. Eyink. A public turbulence database cluster and applications to study lagrangian evolution of velocity increments in turbulence. *Journal of Turbulence*, 2008.
- [86] E. A. Novikov. Random force method in turbulence theory. *Sov. Phys. JETP*, 17:1449–1454, 1963.
- [87] D. Poggi, A. Porporato, L. Ridolfi, J. D. Albertson, and G. G. Katul. The effect of vegetation density on canopy sub-layer turbulence. *Boundary-Layer Meteorology*, 111(3):565–587, Jun 2004.
- [88] H. Xia, N. Francois, H. Punzmann, and M. Shats. Lagrangian scale of particle dispersion in turbulence. *Nature Communications*, 4, 06 2013.

APPENDIX A - SUB-VOLUME FLOW PARAMETERS

The two following tables present the values of the sub-volume parameters that were estimated according to the description in Section II D.

sv	\bar{u} [m/s]	ϵ [W/kg]	η [mm]	τ_η [s]	λ [mm]	Re_λ	H/η
$a1$	0.42	0.201	0.36	0.009	14.14	398	277
$a2$	0.45	0.256	0.34	0.008	13.25	394	295
$a3$	0.49	0.304	0.32	0.007	13.23	428	308
$a4$	0.51	0.244	0.34	0.008	15.35	517	291
$a5$	0.62	0.239	0.34	0.008	19.01	784	290
$b1$	0.36	0.123	0.41	0.011	15.41	369	245
$b2$	0.42	0.193	0.36	0.009	14.18	392	275
$b3$	0.47	0.250	0.34	0.008	14.09	440	293
$b4$	0.50	0.233	0.35	0.008	15.63	523	288
$b5$	0.65	0.305	0.32	0.007	17.63	762	308
$c1$	0.42	0.248	0.34	0.008	12.59	350	292
$c2$	0.43	0.210	0.36	0.008	13.97	397	280
$c3$	0.46	0.286	0.33	0.007	12.82	390	303
$c4$	0.52	0.231	0.35	0.008	16.13	555	287
$c5$	0.62	0.245	0.34	0.008	18.66	766	291
$d1$	0.40	0.175	0.37	0.009	14.18	373	268
$d2$	0.40	0.175	0.37	0.009	14.32	380	268
$d3$	0.47	0.229	0.35	0.008	14.61	454	287
$d4$	0.50	0.218	0.35	0.008	15.99	530	283
$d5$	0.66	0.377	0.31	0.006	16.10	707	325

Table I: Turbulence parameters for each sub-volume for the $Re_\infty = 16 \times 10^3$ case.

sv	\bar{u} [m/s]	ϵ [W/kg]	η [mm]	τ_η [s]	λ [mm]	Re_λ	H/η
$a1$	0.53	0.422	0.30	0.006	12.16	426	334
$a2$	0.54	0.551	0.28	0.005	11.01	399	357
$a3$	0.60	0.703	0.26	0.005	10.68	424	379
$a4$	0.64	0.611	0.27	0.005	12.19	516	366
$a5$	0.83	0.669	0.27	0.005	15.19	839	375
$b1$	0.47	0.257	0.34	0.008	13.80	429	295
$b2$	0.50	0.352	0.31	0.007	12.74	427	319
$b3$	0.60	0.497	0.29	0.005	12.83	516	348
$b4$	0.64	0.487	0.29	0.006	13.79	589	346
$b5$	0.75	0.544	0.28	0.005	15.17	754	356
$c1$	0.52	0.490	0.29	0.006	11.05	379	347
$c2$	0.53	0.412	0.30	0.006	12.46	442	332
$c3$	0.60	0.587	0.28	0.005	11.68	464	363
$c4$	0.64	0.565	0.28	0.005	12.79	546	359
$c5$	0.81	0.706	0.26	0.005	14.49	783	380
$d1$	0.53	0.371	0.31	0.006	13.03	459	323
$d2$	0.52	0.327	0.32	0.007	13.72	478	313
$d3$	0.59	0.524	0.28	0.005	12.28	485	353
$d4$	0.63	0.528	0.28	0.005	12.94	540	353
$d5$	0.88	0.876	0.25	0.004	14.13	830	401

Table II: Turbulence parameters for each sub-volume for the $Re_\infty = 26 \times 10^3$ case.

APPENDIX B - EMPIRICAL ESTIMATION OF AUTOCORRELATION FUNCTIONS

The autocorrelation of the random signals in this work were calculated as follows. Consider the set of $i = 1 \dots N$ random series samples $a_i(\tau)$ of the random variable $a(\tau)$. Generally speaking, the average of $a(\tau)$ and its standard deviation may change with τ , where $\tau = t - t_0$, and t_0 is the time at which the record of a_i began). The average of $a(\tau)$ is defined as

$$\mu(\tau) = \frac{1}{N} \sum_{i=1}^N a_i(\tau) \quad (18)$$

the fluctuations relative to the average are denoted $a_i(\tau)' = a_i(\tau) - \mu(\tau)$, and the standard deviation of $a(\tau)$ is defined

$$\sigma(\tau) = \left[\frac{1}{N} \sum_{i=1}^N a_i'^2(\tau) \right]^{1/2}. \quad (19)$$

Note that these two definitions correspond to the sub-volume average introduced in section II C. Then the autocorrelation of a is calculated as follows

$$\rho(\tau) = \frac{\frac{1}{N} \sum_{i=1}^N [a_i'(0) a_i'(\tau)]}{\sigma(0) \sigma(\tau)} \quad (20)$$

The estimator Eq. (D.3) uses the average and the standard deviations that are allowed to change with τ . As discussed by Guala et al. [44], the Lagrangian trajectories with long tracking time possibly belong to a subset of “weak turbulence”. Consequently, an estimator of ρ that uses a single value μ and σ averaged over all values of τ is a biased estimator that may under predicts $\rho(\tau)$ at long times. Therefore using the definition $\sigma(\tau)$, that changes with τ in Eq.(D.3), prevents this underestimation at long time lags. This issue was discussed in details by Guala et al. [44], where the biased estimator in their paper was denoted Eq. (2.1), and the unbiased estimator Eq. (D.3) here is equivalent to their Eq.(2.6).

The autocorrelation functions were calculated in this article using many samples that were measured during the long experimental runs we have conducted, $\sim 12 - 15$ minutes each. To demonstrate that our estimations of the autocorrelation function and the decorrelation timescale are converged we show in the main panel of Fig. 8 the Lagrangian autocorrelation function with error bars that represent the results of a bootstrapping calculation. Specifically, the dataset of trajectories in sub-volume b3 were divided to three groups and the autocorrelation ρ_{xx} was calculated separately. The error bars show the range of scatter of the results for the three groups and represents a small degree of uncertainty in the range relevant for our study. Furthermore, the inset shows the convergence of T_i that was calculated using subsamples of our data with different sizes. The relative error of T_i is seen to decrease rapidly with the subsample size. Therefore, Fig. 8 demonstrates that the autocorrelation and the decorrelation times were converged in our experiment, and suggests an uncertainty of up to a few percents.

APPENDIX C - FINITE VOLUME EFFECT ON CORRELATION

Since the volume of observation is finite and due to the fact that occupation times of particles within the finite volumes are dependent on their velocity, a natural bias occurs in the estimation of Lagrangian velocity autocorrelation functions in PTV experiments. To minimize this effect on the results shown in this work, the estimation of Lagrangian timescales was performed in this work only on short times, such that most of the particles do not have sufficient time to leave the observation volume. A time scale for the occupation times within a volume of dimension L is

$$T_{vol} = \frac{L}{u'} \quad (21)$$

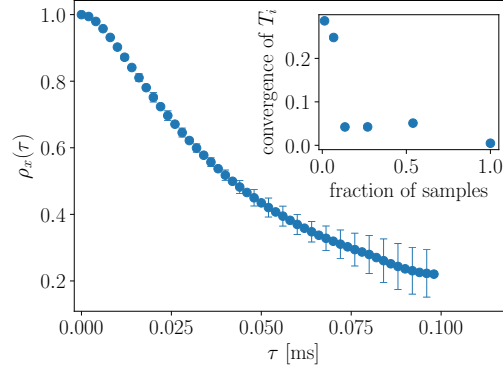


Figure 8: Convergence plots for the autocorrelation function (main panel) and for the decorrelation timescale (inset) for trajectories in sub-volume b3. The error bars in the main panel represent the range of scatter for ρ_{xx} calculated using 3 subsamples of the data. The inset shows the relative error in estimating T_i using subsamples of different sizes.

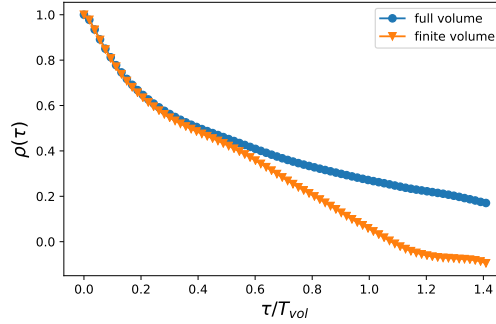


Figure 9: Lagrangian velocity autocorrelation over the full data set compared with trajectories that were truncated to be within finite volume. Plotted against time normalized by the volume timescale, Eq. (21).

with u' being the root mean squared value of particle velocities. In Fig. 9 the Lagrangian autocorrelation function for the x velocity component is presented against time normalized by T_{vol} for the HIT DENS data over two ensembles. The first is the full series of velocities over all trajectories. The second ensemble was obtained by truncating the velocity series of each trajectory such that only values measured within a certain volume of size L were taken to mimic the finite volume effect. The figure shows that for times in the range $\tau < T_{vol}$, the difference that exists between the two autocorrelation estimations is rather small - up to $\sim 5\%$, meaning that the estimation of integral timescales within this range is reasonably close to that using the full range. For this reason, to estimate the Lagrangian integral timescales from the canopy trajectories, we used only time $\tau < 0.5T_{vol}$, with $L = 3\text{mm}$ and u' determined from all samples at a given sub-volume.